ACSNANO

www.acsnano.org

ARTICLE

Kinetically Controlled Sequential Seeded Growth: A General Route to Crystals with Different Hierarchies

Joshua D. Smith, Mattea M. Scanlan, Alexander N. Chen, Hannah M. Ashberry, and Sara E. Skrabalak*

Cite This: *ACS Nano* 2020, 14, 15953–15961

Read Online

ACCESS | Metrics & More | Article Recommendations | Supporting Information

ABSTRACT: The organization of natural materials into hierarchical structures accounts for the amazing properties of many biological systems; however, translating the structural motifs present in such natural materials to synthetic systems remains difficult. Inspired by how nature creates materials, this work demonstrates that kinetically controlled sequential seeded growth is a general bottom-up strategy to prepare hierarchical inorganic crystals with distinct compositions and nanostructured forms. Specifically, 85 distinct hierarchical crystals with different shape-controlled features, compositions, and overall symmetries were readily achieved by altering the kinetics of metal deposition in sequential rounds of seeded growth. These modifications in the deposition kinetics were achieved through simple changes to the reaction conditions (*e.g.*, pH or halide concentration) and dictate whether concave or convex features are produced at specific seed locations, much in the manner that the changing atmospheric conditions account for the hierarchical and symmetrical structures of snow crystals. As such, this work provides a general paradigm for the bottom-up synthesis of hierarchical crystals regardless of inorganic material class.

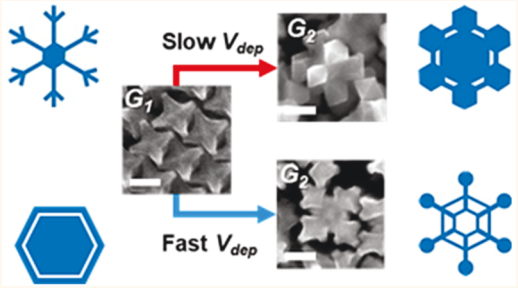

KEYWORDS: *colloidal synthesis, crystal growth, gold nanoparticles, multimetallic nanomaterials, heterogeneous nucleation*

From adhesive properties of gecko feet to the dazzling colors exhibited by *Morpho* butterfly wings, nature's creatures display extraordinary physical and chemical properties that can arise from materials in hierarchical form.[1−4] Yet translating the hierarchical motifs present in nature's materials to engineered nanostructured materials is difficult to achieve by traditional material-processing techniques.[1,5−7] Engineered nanomaterials with hierarchical features are commonly prepared through top-down approaches (*e.g.*, lithography); however, these strategies suffer from (i) complex environments and instrumentation, (ii) difficulties in scalability, and (iii) high production costs.[8−11] In contrast, hierarchical structures produced by biological systems typically arise through bottom-up synthetic processes in which the size, shape, functionality, and crystal structure of the materials are well-defined throughout material formation.[5−7,12,13] Mimicking the templating observed in some biological sysems,[14] hierarchically porous inorganic materials have been synthesized; however, these synthetic inorganic systems often lack fine structural control.[15−17]

Nature gives insight into how bottom-up chemical strategies can be developed to achieve nonbiological hierarchical structures with such fine control. Consider, for example, the formation of snow crystals, which can adopt a range of hierarchical structures.[18−20] The form of a snow crystal begins with heterogeneous nucleation of ice in liquid water droplets around some dust particles in a cloud.[18−20] Once the individual droplet has converted to a snow crystal seed with hexagonal symmetry inherent to ice, water molecules (*i.e.*, monomers) from air directly solidify onto the surface of the snow crystal.[18−20] At low humidity (*i.e.*, low supersaturation), growth of a snow crystal is slow and hexagonal prisms will form.[18−20] In contrast, increasing the humidity (*i.e.*, higher supersaturation) results in faster growth in which snow crystals with complex structures such as needles, dendrimers, and columns are produced that all preserve the hexagonal symmetry of the initial ice crystal.[18−20] Due to the sensitivity of snow crystal growth to the environment, a multitude of crystals are formed as they travel through the ever changing conditions inside a cloud.[18−20]

Received: September 1, 2020
Accepted: October 22, 2020
Published: October 29, 2020

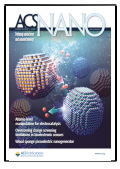

https://dx.doi.org/10.1021/acsnano.0c07384
ACS Nano 2020, 14, 15953–15961

The formation of a snow crystal can be distilled to two main steps: (i) nucleation on a dust particle to create a seed and (ii) growth of a snow crystal from a seed in which changes in growth rate arise from changes in environment (*e.g.*, changes in supersaturation).[18−20] Likewise, nanocrystals can be synthesized through seeded methods in which material preferentially deposits onto preformed crystals (*i.e.*, seeds).[21−24] By controlling the kinetics of adatom addition (v_{dep}) and diffusion (v_{dif}) on seeds, the final crystal shape can be tuned between concave ($v_{dep} \gg v_{dif}$) and convex ($v_{dep} \ll v_{dif}$) morphologies.[21−24] For example, Xia *et al.* demonstrated this concept by systematically changing the reaction temperature during the deposition of Pt onto nanocubic Pd seeds from Na_2PtCl_6.[25] At 160 °C, Pt islands formed on the Pd cubes due to strong Pt−Pt interactions.[21] By increasing the temperature of the reaction to 200 °C, the surface diffusion of Pt atoms (v_{dif}) increases and conformal Pt shells form around the cubes.[25]

The ability to tune between concave and convex structures through kinetically controlled seeded growth provides insight into how nanostructured crystals with different hierarchical forms can be accessed generally by sequential rounds of seeded growth in which the different kinetic regimes are accessed. In fact, hierarchical crystals were achieved by sequential seeded growth previously by simultaneously co-reducing Au and Pd precursors in the presence of shape-controlled Au seeds; however, only one overgrowth motif (branches) was demonstrated.[26] Here, different kinetic regimes are accessed in different rounds of seeded growth, providing access to 85 distinct hierarchical crystals with specific structural features, compositions, and overall symmetries. The general strategy demonstrated here should be applicable to many material classes.

RESULTS AND DISCUSSION

Kinetically Controlled Sequential Seeded Growth. Here, seed-mediated co-reduction (SMCR) is used sequentially as a model synthetic approach to achieve hierarchical crystals with well-defined nanoscale features, compositions, symmetries, and sizes.[26,27] During SMCR, multiple metal precursors are simultaneously co-reduced to deposit metals onto metal nanocrystal seeds of defined shape in the presence of capping agents such as hexadecyltrimethylammonium bromide (CTAB).[27,28] We note here that different capping agents can be introduced to promote the expression of specific facets, but these effects are typically considered a form of thermodynamic control (*i.e.*, they make expression of specific facets energetically more favored).[21,24,27] Although capping agents play a critical role in nanocrystal formation, this work focuses on demonstrating kinetic control by modulating the v_{dep}/v_{dif} ratio. Under fast growth conditions ($v_{dep} \gg v_{dif}$), branched metal nanocrystals are formed, with branching proceeding in the ⟨111⟩ directions in the model system based on Au and Pd deposition on Au seeds.[27,29] In contrast, nanocrystals with convex forms are generated when the growth rate is slowed ($v_{dep} \ll v_{dif}$).[24,28] We leverage this ability to access different kinetic regimes and concave *versus* convex features with SMCR to sequentially build up hierarchical metal crystals with different nanostructured features.

First, 8-branched concave nanocrystals (*i.e.*, octopods) were synthesized by performing SMCR with octahedral Au seeds (Figure S1). Specifically, $HAuCl_4$ and H_2PdCl_4 were co-reduced by L-ascorbic acid (L-AA) to deposit metal onto the octahedra in the presence of either CTAB or hexadecyltrimethylammonium chloride (CTAC) with NaBr. As previously observed, the initial O_h symmetry of the octahedral seeds is translated to the 8-branched octopods (Figure S1).[27] Here, the products formed from each step in sequential SMCR can be assigned a generation (G_n). In this case, G_1 refers to the Au/Pd octopods produced from the first round of SMCR (Figure 1a). Earlier work produced G_2 and G_3 products: 32-branched Au/Pd nanocrystals and 128-branched Au/Pd nanocrystals, respectively, from a second and third round of SMCR under fast growth conditions ($v_{dep} \gg v_{dif}$; Figure 1a).[26] However, slow growth conditions ($v_{dep} \ll v_{dif}$) have not been integrated with sequential SMCR and are central to accessing a diversity of hierarchical forms analogous to the diversity of snow crystals.

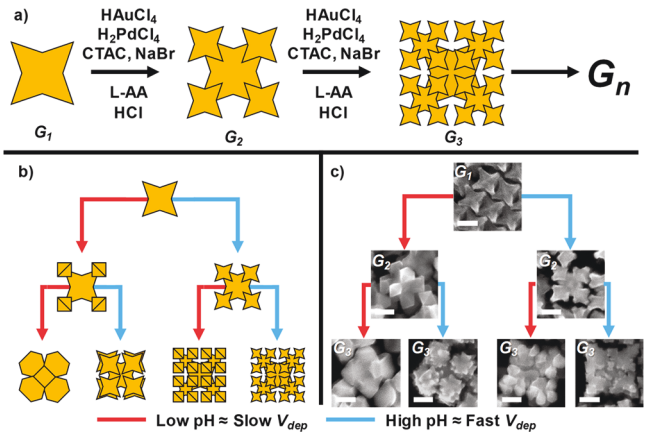

Figure 1. Schematic of (a) sequential seed-mediated co-reduction as a route to hierarchical branched crystals and (b) anticipated changes in morphology from introduction of fast deposition (blue path) or slow deposition (red path) conditions. (c) SEM images of polyhedra-tipped or branch-tipped hierarchical structures obtained through kinetic control. All scale bars are 100 nm.

To demonstrate different hierarchical structures by kinetic control, we found the use of larger octopods as G_1 seeds beneficial on account of the greater spatial separation between their branches (Figures S2 and S3). Given this, octopods with a tip-to-tip length of about 160 nm were used throughout this study as G_1 seeds. Furthermore, growth is expected to occur at the tips of G_1 seeds due to lower coordination numbers of atoms at the branch tips, and in turn, the features at the tips of G_1 can be altered by controlling the rate of metal deposition.[26] Figure 1b displays the different hierarchical forms expected by altering the reduction rate of the metal precursors, with the red pathway indicating slow v_{dep} (arising from slow metal precursor reduction) and the blue pathway indicating fast v_{dep} (arising from fast metal precursor reduction). The rate of metal precursor reduction was modulated by introducing HCl into the growth solution. At higher concentrations of HCl, the halide concentration and pH of the growth solution decrease the rate of metal deposition, resulting in $v_{dep} < v_{dif}$.[30,31] This decrease in metal deposition rate results in hierarchical crystals with polyhedral features at growth sites (*i.e.*, the tips of G_1 seeds). Lower concentrations of HCl result in $v_{dep} \gg v_{dif}$, and in turn, hierarchical crystals with additional branching at growth sites are expected. This pH dependence of metal deposition rate is well-established in the seeded synthesis of Au nanocrystals.[30,31]

https://dx.doi.org/10.1021/acsnano.0c07384
ACS Nano 2020, 14, 15953−15961

Scanning electron microscopy (SEM) images of the G_2 and G_3 products in Figure 1c show that kinetic control can be introduced into sequential seeded growth to obtain hierarchical crystals with different nanostructured forms. At high pH (3.31), G_2 crystals with 32 branched features are produced, with 4 branches emerging from each branch of an octopodal G_1 seed and proceeding in ⟨111⟩ directions. In contrast, lowering the pH to 2.38 decreases the rate of metal deposition, and hierarchical crystals with convex forms at the tips of the octopodal G_1 seeds are produced. Note, the pH of the solution was measured prior to the addition of G_1 seeds. Looking closely, the structures at the tips of the G_1 seeds adopt octahedral morphologies, indicating that overgrowth can occur at specific seed features with shape control. As the spatial arrangement of the overgrowth is governed by the underlying symmetry of the initial seeds, this demonstration reflects a potentially general means of arranging shape-controlled nanocrystal features in 3-D space.

Significantly, these structural motifs can be translated into G_3 products by performing another round of SMCR with G_2 structures as seeds. The right path of Figure 1c shows the hierarchical crystals with 128 branches that are produced under high pH (*i.e.*, fast deposition) conditions from the 32-branched G_2 seeds; as discussed in the original publication of these structures, the assignment of 128 branches is idealized as some branches grow into one another due to crowding but is based on the preference of growth in ⟨111⟩ directions.[26] In contrast, low pH (slow v_{dep}) conditions places polyhedra at the 32 branches of these G_2 seeds. SEM images in Figure S4 demonstrate that these design motifs are present in many other G_3 products.

Interestingly, hyperbranched and enlarged 8-tipped polyhedral structures are grown by performing sequential SMCR onto the G_2 seeds with octahedral-like structures at the tips of G_1 seeds depending on the reaction pH (left path of Figure 1c). The hyperbranched structures are consistent with the higher pH conditions favoring $v_{dep} \gg v_{dif}$. In preceding research, 4 branches are observed to emerge from each vertex of a polyhedron.[32] As there are 8 octahedra at the tips of the crystals, with 5 of the 6 vertices being exposed, the preferences for branch growth in the ⟨111⟩ direction theoretically gives rises to 160-branched structures. However, imperfections in the octahedra result in slightly more, or less, branches. In contrast, the lower pH conditions should favor $v_{dep} < v_{dif}$, encouraging enlargement of the polyhedral shapes of the original G_2 seeds with 8 octahedral-like structures. Electron micrographs in Figure S4 further show that hierarchical crystals with these design motifs can be synthesized in good yield. Similar to how snow crystals maintain the hexagonal symmetry of their initial seeds, these crystals maintain the initial quasi-O_h symmetry throughout subsequent generations, with subtle differences in branches breaking complete symmetry transfer.

Additional SEM characterization of the G_2 structures in Figure 2 shows the difference between hierarchical crystals tipped with additional branches *versus* polyhedra. Large field-of-view SEM images in Figure 2a,f and Figure S5 show that hierarchical crystals are generated in high yield. Transmission electron microscopy (TEM) images in Figure 2b and a tilt study in Figure S6 show that 4 branches emerge from the tips of the G_1 octopods. Analysis of G_2 crystals synthesized at lower pH indeed reveals that octahedral structures grow on the tips of G_1 octopodal seeds (Figure 2f–h and Figure S6). Scanning transmission electron microscopy (STEM) coupled with

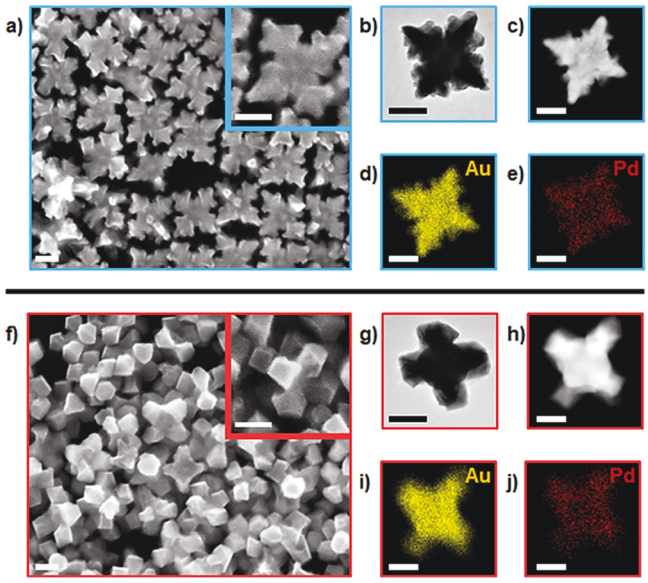

Figure 2. SEM images with single particle insets of (a) 32-branched and (f) polyhedra-tipped crystals obtained from performing seed-mediated co-reduction onto Au/Pd octopods. (b,g) TEM and (c,h) STEM images of a 32-branched and polyhedra-tipped crystals. Elemental maps by STEM-EDS of Au (yellow) and Pd (red) of the respective products are presented in d,e and i,j. All scale bars are 100 nm.

energy-dispersive X-ray spectroscopy (EDS) and powder X-ray diffraction (XRD) reveal that Au and Pd are alloyed in the final crystals (Figure 2d,e,i,j and Figure S7). This composition is ultimately important to the properties displayed by the nanocrystals.

Au nanomaterials are finding use in many applications; however, these materials often suffer from poor temporal and thermal stability due to the high surface mobility of Au atoms.[33−36] Here, hierarchical crystals prepared in the manner that produced the samples in Figure 2a,f show no major structural changes after storage in aqueous solution for 22 months as imaged by SEM (Figure S8). Furthermore, these crystals maintained their respective forms after being heated at 100 °C in water for 1 h (Figure S8). This stability is consistent with the Au/Pd composition, as observed in studies of the G_1 octopodal nanocrystals.[21,34]

To this point, this work has focused on qualitatively analyzing the kinetics of the reaction by associating a branched or polyhedral-tipped structure with fast v_{dep} or slow v_{dep}, respectively. To provide quantitative understanding of the process, time studies were conducted (Figure 3a,b) in which bis(*p*-sulfonatophenyl)phenylphosphine dihydrate dipotassium salt (BSPP) was introduced to quench the growth from the G_1 seeds into the G_2 products generated at high and low pH and at time points between 10 s and 3600 s (1 h).[29,36,37] Results of the time study are presented in Figure 3, in which the products from 10, 120, 300, 1800, and 3600 s were analyzed by SEM (Figure 3a,b) and the change in the tip-to-tip length is plotted *versus* time (see Figure 3C). Furthermore, these data were coupled with *in situ* ultraviolet−visible−near-infrared (UV−vis-NIR) spectroscopy of the growth solution in which a spectrum was acquired from 300 to 1300 nm every 158 s and allows the localized surface plasmon resonance (LSPR) to be monitored as changes in crystals' size, shape, and composition

https://dx.doi.org/10.1021/acsnano.0c07384
ACS Nano 2020, 14, 15953−15961

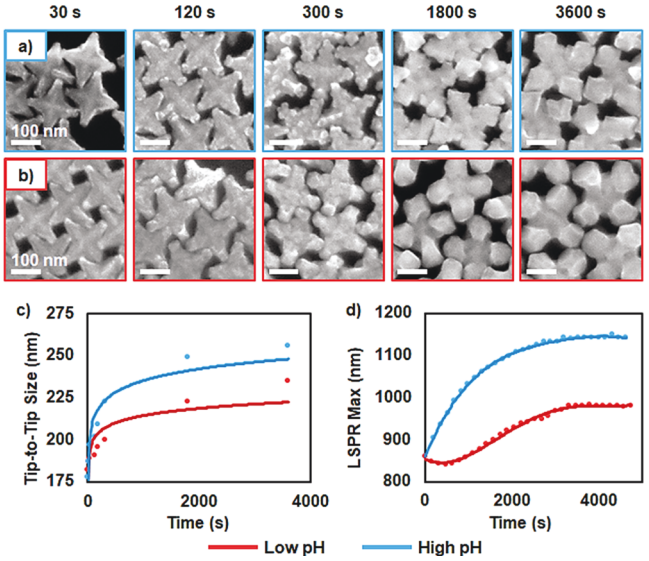

Figure 3. SEM images of hierarchical crystals obtained at different time points under (a) high pH (blue) and (b) low pH (red) conditions. Plots of the (c) tip-to-tip size and (d) LSPR maximum *versus* time (seconds) acquired through size analysis and UV−vis−NIR spectroscopy, respectively. Unless noted, all scale bars are 100 nm. Red and blue plots refer to low and high pH, respectively.

result in shifts in LSPR position and profile.[27,38,39] Results for this work are presented in Figure 3 and Figures S9−S14.

The SEM images of products obtained under high and low pH conditions show distinct overgrowth processes, consistent with different kinetics (Figure 3). As the reactions progress to 300 s, the topographies of the structures are quite different, where the surfaces of crystals grown at higher pH are rougher initially than those grown at lower pH. The metal islands creating the rough topographies at higher pH appear to coalesce into branches as the reaction proceeds, whereas smooth polyhedra grow at lower pH. Considering metal deposition on surfaces, islands are commonly observed at high concentrations of precursors and low temperatures, consistent with high supersaturation/faster deposition processes and slow adatom surface diffusion.[40−43] In contrast, layer-by-layer growth is commonly observed at low concentrations of precursors and high temperatures, consistent with low supersaturation/slower deposition and fast adatom surface diffusion.[40−42] Here, we propose that altering the pH of the solutions allows us to govern whether island or layer-by-layer overgrowth pathways occur. Looking at products synthesized at an even lower pH (1.57), convex crystals are observed (Figure S10). This result further supports that different growth modes can be achieved by modulating the pH of the solution.

The overall size (tip-to-tip length) and tip widths of the crystals were measured at each time point (Figure 3c). Measurements are summarized in Table S1, with the dimensions plotted *versus* time in Figure 3c. At high pH, the tip-to-tip length of the crystals increases in size 1.50× faster than the crystals grown at lower pH (Figure 3c and Figure S11). Looking at Figures S11 and S12 and Table S2, the widths of the tips increase at similar rates (high pH tip increase 1.08× faster than low pH). This result is interesting but expected given that the high energy surface sites at the tips of octopods are preferred under kinetically controlled conditions.[25,31] Generally speaking, these results demonstrate that the size of crystals grows more rapidly at high pH when compared to crystals synthesized at low pH.

The difference in rates of size change as a function of pH is further supported by the UV−vis−NIR time study presented in Figure 3d and Figures S13 and S14. When considering the LSPR maximum of a branched nanocrystal, increasing the size and sharpness of a branch tip results in a red shift of LSPR wavelength.[38,39,44] When comparing the LSPR wavelength position as a function of time for both syntheses (Figure 3d and Figure S13), the LSPR red shifts 1.26× faster for crystals synthesized under high pH conditions when compared to the crystals synthesized under low pH conditions (see Figure S14 and Table S2). We do note that this is not a fully quantitative value due to changes in both size and tip sharpness as well as composition.[38,39,44] Regardless, these results do indeed support the size analysis.

To understand the kinetics of metal deposition, the concentration of Au and Pd in the supernatant was analyzed at different time points by inductively coupled plasma mass spectrometry (ICP-MS). Notably, metal decreases more rapidly under high pH conditions (blue plots) when compared to that at low pH conditions (red plots). When considering the linear relation of the plots of the natural log of metal concentration over time (Figure 4c,d and Table S2), this

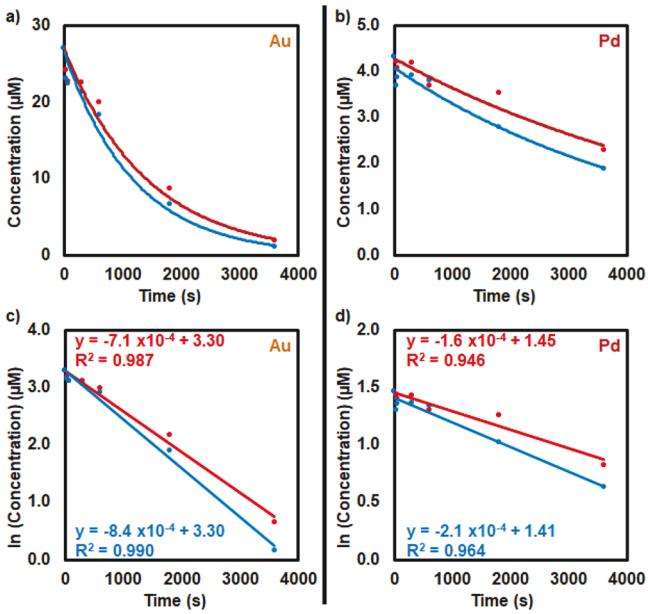

Figure 4. Graphs of metal precursor concentration (μM) *versus* time (seconds) acquired by ICP-MS. The concentration of (a) gold and (b) palladium precursor remaining in solution at different time points of the reaction. Plots in (c,d) are the natural log of metal concentration compared to the reaction time with linear fit to the plots. The good agreement is represented by displaying the equation of the fit line and R^2 value as insets in plots c and d. This agreement is indicative of first-order reaction kinetics. Reactions ran at high pH and low pH are colored red and blue, respectively.

analysis supports assignment of first-order reactions. This analysis is in good agreement with recent literature in which the reduction of the Au and Pd precursors followed a pseudo-first-order rate law.[45,46] The rates of the Au precursor reduction were found to be −0.00084 and −0.00071 s^{-1} for high pH and low pH, respectively. Similarly, the rates of the Pd precursor reduction were found to be −0.00021 and −0.00016

https://dx.doi.org/10.1021/acsnano.0c07384
ACS Nano 2020, 14, 15953−15961

s^{-1} for high pH and low pH conditions. By decreasing the rate of precursor reduction, the rate of v_{dep} can be effectively reduced given that the temperature, pressure, viscosity, solvent, *etc.* are constant.[24,47] Effectively, performing SMCR at high pH results in scenario in which $v_{dep} \gg v_{dif}$, and in turn, crystals with concave hierarchical forms are observed. In contrast, performing SMCR at low pH reduced the rate of deposition (*i.e.*, $v_{dep} \ll v_{dif}$); thus, crystals with convex hierarchical forms are observed. These results support the more qualitative analyses by SEM topology and size as well as UV−visible−NIR spectroscopy, as the Au and Pd precursors are reduced 1.18× and 1.31× faster at a higher pH.

From the discussion above, introducing kinetic control into sequential SMCR is a viable route to synthesize crystals with tailorable nanoscale features. Reflecting back on the formation of snow crystals, minor changes in growth conditions can result in significant changes in crystal morphology.[18−20] Similarly, the kinetic analysis reveals that small changes in reaction kinetics result in significant changes in the hierarchical forms. This result will be explored further in the following section. Given that these results are rooted in fundamental principles of crystal growth, this work is expected to be applicable to other inorganic material systems.

Controlling the Nanoscale Features of Hierarchical Crystals. Similar to the results above, the final morphology a snow crystal adopts is extremely sensitive to the humidity and temperature.[18−20] For instance, a simple change in 2 °C can drive a snow crystal to adopt a needle-like *versus* a plate-like form.[18−20] To this point, this study has only looked at two conditions: high pH and low pH. At high pH (fast v_{dep}), branched hierarchical crystals are formed, and polyhedra-tipped hierarchical crystals are formed at slow v_{dep}. Different ratios of v_{dep} to v_{dif} should produce intermediate crystal shapes not yet achieved.[24,47,48] Thus, to access hierarchical crystals with fine control over nanoscale tip features, different concentrations of HCl and NaBr were added to the growth solution. Here, NaBr is leveraged as an additional synthetic lever to modulate the rate of metal deposition. Through Le Chatelier's principle, increasing the concentration of Br^- in solution promotes the ligand exchange of chloride metal salts to their bromide analogues. This change in local ligand environment is leveraged to alter the reduction potentials of the metal precursors.[28,30,31,48,49] For instance, the rate of reduction for $AuBr^{4-}$ to Au is expected to be slower than that of $AuCl_4^-$.[50] Given the discussion above, polyhedral-tipped hierarchical crystals are expected to be achieved at high Br^- concentrations, with branched crystals achieved at lower Br^- concentrations.

SEM images in Figure 5 show the results of changing the concentration of HCl and Br^-. To understand the influence of NaBr, CTAB was replaced with CTAC and variable NaBr. The concentration of HCl solution increases down a column, with row A corresponding to 0 mM HCl, row B corresponding to 12.5 mM HCl, row C corresponding to 25 mM HCl, and row D corresponding to 50 mM HCl. Although the pH of the growth solutions in rows A−D in column 1 range from 3.31 to 2.38, the pH of each growth solution was not measured. Given this, the following discussion will focus on the concentration of HCl. Similarly, the concentration of NaBr solution added decreases across a row from left to right, where column A corresponds to 400 mM NaBr solution, column B corresponds to 350 mM NaBr solution, column A corresponds to 300 mM NaBr solution, and column A corresponds to 150 mM NaBr solution.

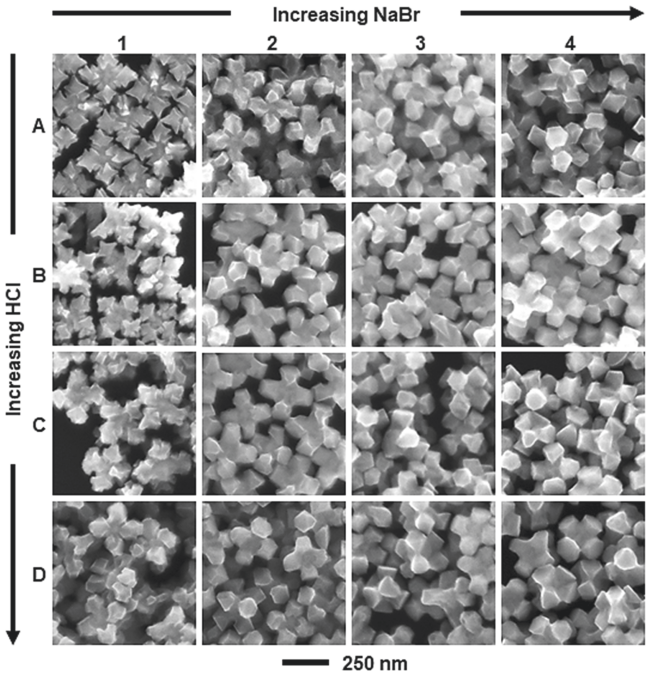

Figure 5. SEM images of hierarchical crystals obtained by decreasing the pH and decreasing the concentration of NaBr. The concentration of added HCl in rows A, B, C, and D was 0, 12.5, 25, and 50 mM. The concentration of NaBr solution was 400, 350, 300, and 150 mM for columns 1, 2, 3, and 4, respectively.

Similar to the results in Figure 1, the gradual decreasing of HCl results in the hierarchical crystals transitioning from branched-tipped to polyhedral-tipped crystals. Likewise, increasing the concentration of NaBr in solution results in the formation of polyhedral features at the tips (Figure 5, row A) with well-defined octahedral-like structures present at high concentrations of NaBr and branched features at lower NaBr. This observation is in good agreement that the rate of metal deposition decreases by increasing the concentration of NaBr.[28,30,31,49] Column 4 in Figure 5 demonstrates that shape control at the tips of hierarchical crystals is possible in sequential SMCR in which plate-like structures form at high Br^- and low concentrations of HCl. Interestingly, octahedral-like structures can be achieved at high Br^- and high concentrations of HCl. Furthermore, column 1 of Figure 5 demonstrates that the branch structures at the tip can be tuned by controlling similar conditions. Interestingly, substituting CTAB for CTAC/NaBr results in similar structures but with differences in tip sharpness being evident (Figure S15). Here, we note that the conditions that produced the samples in Figure S15 A3 (branched form) and Figure S15 D3 (polyhedral form) are the same used for samples in Figures 1 and 2.

Although the above demonstrated hierarchical crystals are already a significant advance in themselves, materials with specific and well-defined compositions are desirable for many applications.[51−54] SMCR has been used to synthesize materials with diverse compositions;[55−58] however, changing the composition can directly influence the final structure. As previously discussed, the high surface mobility of Au atoms in monometallic Au nanocrystals commonly leads to significant instability of crystal shape.[59−61] Recall, the final morphology of

https://dx.doi.org/10.1021/acsnano.0c07384
ACS Nano 2020, 14, 15953−15961

the tip feature is dependent on the ratio of v_{dep} to v_{dif}.[24] Here, the high surface mobility of Au is leveraged to demonstrate that composition is an additional synthetic lever to manipulate the nanostructuring of the hierarchical crystals. By increasing the content of Au, the rate of surface diffusion is expected to increase, resulting in polyhedral tip features.

Figure 6 shows SEM images of the results of changing the Au/Pd deposition ratio as a function of HCl concentration.

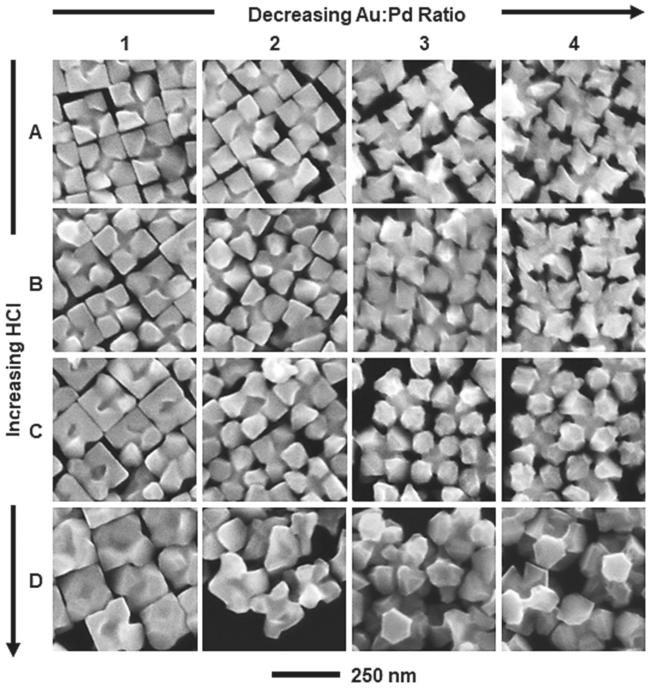

Figure 6. SEM images of hierarchical crystals obtained by decreasing the pH and decreasing ratio of Au/Pd precursors. The concentration of added HCl in rows A, B, C, and D was 0, 12.5, 25, and 50 mM. The Au/Pd ratio in solution was 100:1, 50:1, 10:1, and 5:1 for columns 1, 2, 3, and 4, respectively.

The concentration of HCl solution decreases down a column with row A corresponding to 0 mM HCl, row B corresponding to 12.5 mM HCl, row C corresponding to 25 mM HCl, and row D corresponding to 50 mM HCl. Different ratios of Au/Pd metal salts were deposited by maintaining the concentration of $HAuCl_4$ solution at 10 mM and altering the concentration of H_2PdCl_4 to 0.1 mM for column 1, 0.2 mM for column 2, 1.0 mM for column 3, and 2.0 mM for column 4. Note, this experiment was performed using CTAB as a capping agent.

The modulation of the metal salt ratio in the growth solution provides a synthetic handle to tune both the composition and tip structures. For instance, features at the tip of hierarchical crystals appear to adopt a pyramidal morphology at high concentrations of HCl and low Pd content (Figure 6A1). In contrast, increasing the concentration of Pd results in the formation of branched structures. Given that the surface diffusion of Au is faster than that of Pd and Au deposits primarily first,[36] we propose that the larger Au/Pd ratio results in polyhedral-like structures by allowing depositing atoms to adopt more thermodynamically favored positions. Qualitatively, this hypothesis is supported as the v_{dep} decreases down a column, and in turn, the concavity of the crystals decreases. As observed in Figure 6, increasing the amount of HCl in the system results in the formation of polyhedral features in which the structural features are dependent on both the composition and metal deposition ratios. For instance, row D of Figure 6 shows that the tip features depend on the Au/Pd ratio, with plate-like morphologies being observed at 10:1 Au/Pd ratio (Figure 6D3). Interestingly, performing sequential SMCR at low concentrations of Pd salts and high concentration of HCl results in the growth of crystals into more thermodynamically favored cubic structures. In brief, the Au/Pd ratio is used as a bifunctional synthetic handle to modulate the composition and structure of the features at the tips of branched seeds.

Going beyond the Au and Pd system, hierarchical crystals with different amounts of Au, Pd, and Ag were prepared by co-reducing different ratios of Au/Ag/Pd salts in the presence of CTAB and G_1 seeds (Figure S16). Although it is feasible to achieve hierarchical forms with different compositions, it is important that one considers the deposition and surface diffusion rates of each metal. Excitingly, these results demonstrate that hierarchical crystals with a variety of multimetallic compositions can be readily achieved. Overall, the development of multimetallic hierarchical crystals with different metals, and metal ratios, unlocks many opportunities to design structures for diverse applications.

Beyond Hierarchical Crystals with Quasi-O_h Symmetry. Reflecting on the formation of snow crystals, they commonly adopt morphologies with six-fold symmetry.[18−20] This symmetry is attributed to the normal form of ice adopting a hexagonal crystal structure.[20] However, the introduction of twin planes and grain boundaries can play a significant role in the growth and final morphology of snow crystals.[20,62,63] Similarly, introducing twin planes into nanocrystals provides a route to structures with symmetries not readily available from single-crystalline face-centered cubic metals.[62,63] Here, we investigated the growth of hierarchical crystals from 10-branched decahedra that have five twin planes.

Results from this work are presented in Figure 7 and Figures S17 and S18. Scanning electron micrographs in Figure 7a,b clearly display that decahedra (seeds, Figure 7a),[63] and 10-branched decahedra (G_1, Figure 7b)[29] were successfully prepared in good yield. Higher level characterization of the G_2 structures in Figure 2 shows the difference between hierarchical crystals tipped with additional branches *versus* polyhedra. Electron micrographs in Figure 7c,d,h,i do indeed show that hierarchical crystals with branched and polyhedral structures can be synthesized by growing structures under high and low pH conditions (pH of 3.09 and 2.72, respectively). Similar to 32-branched hierarchical crystals, TEM and SEM images in Figure 7c and Figure S17 appear to have 4 branches growing from each of the 10 branches of the seed. Yet, the total number of branches appears to exceed the theoretically expected 40 branches. Similarly, polyhedra can be found at the tips of each the 10 branches; however, the number of polyhedra exceeds the expected 10 (Figure 7h and Figure S17). We attribute the difference in number of branches/polyhedra to (i) atomic imperfections in crystallographically equivalent sites and (ii) growth around the equatorial plane of the branched decahedra. STEM-EDS elemental mapping reveals that both Au and Pd are incorporated into the final nanocrystals (Figure 7e−g,j−l).

Similar to hierarchical crystals with quasi-O_h symmetry, the nanoscale features at the tips of branched decahedra can be tuned by altering the concentration of NaBr and the concentration of HCl in the solution (Figure S18). In general,

https://dx.doi.org/10.1021/acsnano.0c07384
ACS Nano 2020, 14, 15953−15961

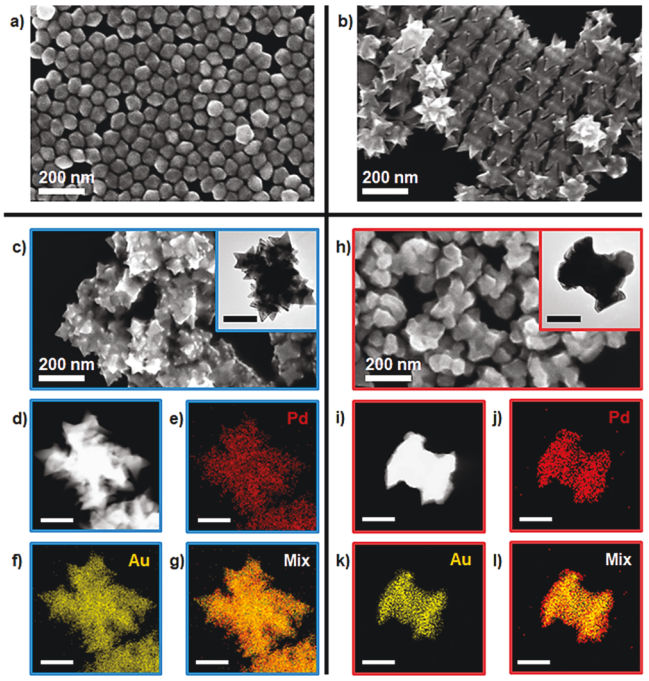

Figure 7. SEM images of (a) decahedral seeds and (b) G_1 branched decahedra. SEM images of (c) 40 branched crystals and (h) 10 polyhedral structures at the tips of the crystals with inset TEM images obtained under high pH (blue outline) and low pH (red outline) conditions. STEM images and elementals maps are presented in (d–g) for a 40 branched crystal and (i–l) for a 10 polyhedral-tipped crystal. For maps, Pd distribution is represented in red and Au is represented in yellow. Unless noted, all scale bars are 100 nm.

hierarchical crystals with quasi-D_{5h} symmetry can be synthesized using seeds with D_{5h} symmetry. Although not explored in this work, it can be easily envisioned that hierarchical crystals with I_h, D_{3h}, T_d, D_{4h}, and additional symmetries can be readily synthesized through sequential seed-mediated growth simply by changing the symmetry of the initial building blocks.[23,27,29]

CONCLUSION

Here, sequential seed-mediated growth is demonstrated as a versatile route to synthesize hierarchical crystals with precise nanostructural features and compositions. By introducing kinetic control into sequential seed-mediated growth strategies, crystals with specific structural and compositional features could be prepared by simply altering the pH or halide concentration of the growth solution. Through modulation of these two synthetic parameters, over 85 distinct inorganic hierarchical crystals have been synthesized in this work. As this demonstration is grounded in fundamental concepts of crystal growth, this synthetic strategy is expected to be transferable to many other material systems that include metal oxides, metal chalcogenides, and more.[64−66] Given the need to precisely arrange materials in 3-D space for a variety of applications, we envision generalizing this strategy to achieve heterostructures as other material systems are demonstrated.

MATERIALS AND METHODS

Leveraging the principles of seed-mediated growth, kinetically controlled sequential seeded growth can be distilled to a few general steps. First, a growth solution is prepared in which some metal monomer is deposited onto preformed nanoparticle seeds. This step generates G_1 nanostructures that can be used as are or as seeds for a subsequent round of seed-mediated growth. To generate G_2 structures, another growth solution is prepared to generate metal monomers for deposition onto G_1 seeds. This process can be repeated to synthesize multiple generation of hierarchical crystals. By introducing kinetic control into each step, the nanofeatures can be readily tuned. Given the basis of this process in crystal growth theory, this process is expected to be translatable to many other systems.

More specific to this system, sequential SMCR is leveraged as a model system to generate multimetallic hierarchical crystals.[26] In brief, an aqueous solution containing metals salts, a specific concentration of surfactant, and some amount of HCl is prepared in a glass vial. Using L-ascorbic acid, metal salts are simultaneously co-reduced to generate metals for deposition in the presence of preformed seeds. For hierarchical crystals, 8-branched octopodal nanocrystals are used to achieve hierarchical crystals with a quasi-O_h symmetry. To achieve hierarchical crystals with a quasi-D_{5h} symmetry, 10-branched decahedra are used as seeds. The hierarchical crystals were centrifuged and dispersed in 3 mL of nanopure water. For successive generations, the process above was repeated with a certain volume of the previously synthesized hierarchical crystals.

A complete description of chemicals, synthetic procedures, and characterization techniques can be found in the Supporting Information.

ASSOCIATED CONTENT

Supporting Information

The Supporting Information is available free of charge at https://pubs.acs.org/doi/10.1021/acsnano.0c07384.

A list of chemicals, characterization techniques, synthetic protocols, and supporting figures (additional electron micrographs of different samples, tilt studies of samples, absorbance spectra of time studies, schematics, analysis of multimetallic samples, and tables summarizing specific results) (PDF)

AUTHOR INFORMATION

Corresponding Author

Sara E. Skrabalak − *Department of Chemistry, Indiana University, Bloomington, Indiana 47405, United States;* orcid.org/0000-0002-1873-100X; Email: sskrabal@indiana.edu

Authors

Joshua D. Smith − *Department of Chemistry, Indiana University, Bloomington, Indiana 47405, United States*

Mattea M. Scanlan − *Department of Chemistry, Indiana University, Bloomington, Indiana 47405, United States*

Alexander N. Chen − *Department of Chemistry, Indiana University, Bloomington, Indiana 47405, United States*

Hannah M. Ashberry − *Department of Chemistry, Indiana University, Bloomington, Indiana 47405, United States*

Complete contact information is available at: https://pubs.acs.org/10.1021/acsnano.0c07384

Author Contributions

J.S. and S.S were responsible for design of this study. J.S was responsible for kinetic analysis, synthesis of hierarchical crystals, and characterization of materials. M.S. was responsible for the synthesis of hierarchical crystals from pentatwinned seeds and tilt studies. J.S. and A.C. were responsible for higher level electron microscopy. H.A. aided in powder XRD. The manuscript was written through contributions of all authors.

https://dx.doi.org/10.1021/acsnano.0c07384
ACS Nano 2020, 14, 15953−15961

All authors have given approval to the final version of the manuscript.

Notes

The authors declare no competing financial interest.

ACKNOWLEDGMENTS

This work was funded by the National Science Foundation (NSF-CHE No. 1904499) and Research Corporation for Scientific Advancement (Frontiers in Research Excellence Award). J.S. recognizes a Ph.D. fellowship from the Indiana Space Grant Consortium. The authors thank the Nanoscale Characterization Facility (Dr. Yi Yi and Dr. Jun Chen), Electron Microscopy Center (Dr. David Morgan, Dr. Berry Stein, and Dr. Xun Zhan), and Stable Isotope Research Facility (Dr. Shelby Rader) for their continued support of this work. The authors also thank Sarah Severson and Ayanna Culmer-Gilbert for some initial observations that inspired the design of this study.

REFERENCES

(1) Fratzl, P.; Weinkamer, R. Nature's Hierarchical Materials. *Prog. Mater. Sci.* **2007**, *52*, 1263−1334.
(2) Liu, K.; Du, J.; Wu, J.; Jiang, L. Superhydrophobic Gecko Feet with High Adhesive Forces towards Water and Their Bio-Inspired Materials. *Nanoscale* **2012**, *4*, 768−772.
(3) Vukusic, P.; Sambles, J. R.; Lawrence, C. R.; Wootton, R. J. Quantified Interference and Diffraction in Single Morpho Butterfly Scales. *Proc. R. Soc. London, Ser. B* **1999**, *266*, 1403−1411.
(4) He, J.; Villa, N. S.; Luo, Z.; An, S.; Shen, Q.; Tao, P.; Song, C.; Wu, J.; Deng, T.; Shang, W. Integrating Plasmonic Nanostructures with Natural Photonic Architectures in Pd-Modified Morpho Butterfly Wings for Sensitive Hydrogen Gas Sensing. *RSC Adv.* **2018**, *8*, 32395−32400.
(5) Fratzl, P. Biomimetic Materials Research: What Can We Really Learn from Nature's Structural Materials? *J. R. Soc., Interface* **2007**, *4*, 637−642.
(6) Wegst, U. G. K.; Bai, H.; Saiz, E.; Tomsia, A. P.; Ritchie, R. O. Bioinspired Structural Materials. *Nat. Mater.* **2015**, *14*, 23−36.
(7) Gong, C.; Sun, S.; Zhang, Y.; Sun, L.; Su, Z.; Wu, A.; Wei, G. Hierarchical Nanomaterials *via* Biomolecular Self-Assembly and Bioinspiration for Energy and Environmental Applications. *Nanoscale* **2019**, *11*, 4147−4182.
(8) Gardner, D. F.; Evans, J. S.; Smalyukh, I. I. Towards Reconfigurable Optical Metamaterials: Colloidal Nanoparticle Self-Assembly and Self-Alignment in Liquid Crystals. *Mol. Cryst. Liq. Cryst.* **2011**, *545*, 3−21.
(9) Biswas, A.; Bayer, I. S.; Biris, A. S.; Wang, T.; Dervishi, E.; Faupel, F. Advances in Top−down and Bottom−up Surface Nanofabrication: Techniques, Applications & Future Prospects. *Adv. Colloid Interface Sci.* **2012**, *170*, 2−27.
(10) Salaita, K.; Wang, Y.; Mirkin, C. A. Applications of Dip-Pen Nanolithography. *Nat. Nanotechnol.* **2007**, *2*, 145−155.
(11) George, S. M. Atomic Layer Deposition: An Overview. *Chem. Rev.* **2010**, *110*, 111−131.
(12) Gangwar, T.; Schillinger, D. Microimaging-Informed Continuum Micromechanics Accurately Predicts Macroscopic Stiffness and Strength Properties of Hierarchical Plant Culm Materials. *Mech. Mater.* **2019**, *130*, 39−57.
(13) Aizenberg, J.; Fratzl, P. New Materials through Bioinspiration and Nanoscience. *Adv. Funct. Mater.* **2013**, *23*, 4398−4399.
(14) Seitz, O. Templated Chemistry for Bioorganic Synthesis and Chemical Biology. *J. Pept. Sci.* **2019**, *25*, No. e3198.
(15) Li, C.; Iqbal, M.; Lin, J.; Luo, X.; Jiang, B.; Malgras, V.; Wu, K. C.-W.; Kim, J.; Yamauchi, Y. Electrochemical Deposition: An Advanced Approach for Templated Synthesis of Nanoporous Metal Architectures. *Acc. Chem. Res.* **2018**, *51*, 1764−1773.
(16) Yang, X.-Y.; Chen, L.-H.; Li, Y.; Rooke, J. C.; Sanchez, C.; Su, B.-L. Hierarchically Porous Materials: Synthesis Strategies and Structure Design. *Chem. Soc. Rev.* **2017**, *46*, 481−558.
(17) Li, C.; Iqbal, M.; Jiang, B.; Wang, Z.; Kim, J.; Nanjundan, A. K.; Whitten, A. E.; Wood, K.; Yamauchi, Y. Pore-Tuning to Boost the Electrocatalytic Activity of Polymeric Micelle-Templated Mesoporous Pd Nanoparticles. *Chem. Sci.* **2019**, *10*, 4054−4061.
(18) Yokoyama, E.; Kuroda, T. Pattern Formation in Growth of Snow Crystals Occurring in the Surface Kinetic Process and the Diffusion Process. *Phys. Rev. A: At., Mol., Opt. Phys.* **1990**, *41*, 2038−2049.
(19) Frank, F. C. Snow Crystals. *Contemp. Phys.* **1982**, *23*, 3−22.
(20) Libbrecht, K. G. The Physics of Snow Crystals. *Rep. Prog. Phys.* **2005**, *68*, 855−895.
(21) Xia, Y.; Xiong, Y.; Lim, B.; Skrabalak, S. E. Shape-Controlled Synthesis of Metal Nanocrystals: Simple Chemistry Meets Complex Physics? *Angew. Chem., Int. Ed.* **2009**, *48*, 60−103.
(22) Niu, W.; Zhang, L.; Xu, G. Seed-Mediated Growth of Noble Metal Nanocrystals: Crystal Growth and Shape Control. *Nanoscale* **2013**, *5*, 3172−3181.
(23) Xia, Y.; Gilroy, K. D.; Peng, H.-C.; Xia, X. Seed-Mediated Growth of Colloidal Metal Nanocrystals. *Angew. Chem., Int. Ed.* **2017**, *56*, 60−95.
(24) Xia, Y.; Xia, X.; Peng, H.-C. Shape-Controlled Synthesis of Colloidal Metal Nanocrystals: Thermodynamic *versus* Kinetic Products. *J. Am. Chem. Soc.* **2015**, *137*, 7947−7966.
(25) Xia, X.; Xie, S.; Liu, M.; Peng, H.-C.; Lu, N.; Wang, J.; Kim, M. J.; Xia, Y. On the Role of Surface Diffusion in Determining the Shape or Morphology of Noble-Metal Nanocrystals. *Proc. Natl. Acad. Sci. U. S. A.* **2013**, *110*, 6669−6673.
(26) Weiner, R. G.; Skrabalak, S. E. Metal Dendrimers: Synthesis of Hierarchically Stellated Nanocrystals by Sequential Seed-Directed Overgrowth. *Angew. Chem.* **2015**, *127*, 1197−1200.
(27) Weiner, R. G.; Kunz, M. R.; Skrabalak, S. E. Seeding a New Kind of Garden: Synthesis of Architecturally Defined Multimetallic Nanostructures by Seed-Mediated Co-Reduction. *Acc. Chem. Res.* **2015**, *48*, 2688−2695.
(28) DeSantis, C. J.; Sue, A. C.; Bower, M. M.; Skrabalak, S. E. Seed-Mediated Co-Reduction: A Versatile Route to Architecturally Controlled Bimetallic Nanostructures. *ACS Nano* **2012**, *6*, 2617−2628.
(29) Smith, J. D.; Bladt, E.; Burkhart, J. A. C.; Winckelmans, N.; Koczkur, K. M.; Ashberry, H. M.; Bals, S.; Skrabalak, S. E. Defect-Directed Growth of Symmetrically Branched Metal Nanocrystals. *Angew. Chem., Int. Ed.* **2020**, *59*, 943−950.
(30) Luty-Błocho, M.; Wojnicki, M.; Fitzner, K. Gold Nanoparticles Formation *via* Au(III) Complex Ions Reduction with l-Ascorbic Acid. *Int. J. Chem. Kinet.* **2017**, *49*, 789−797.
(31) Personick, M. L.; Mirkin, C. A. Making Sense of the Mayhem behind Shape Control in the Synthesis of Gold Nanoparticles. *J. Am. Chem. Soc.* **2013**, *135*, 18238−18247.
(32) DeSantis, C. J.; Skrabalak, S. E. Core Values: Elucidating the Role of Seed Structure in the Synthesis of Symmetrically Branched Nanocrystals. *J. Am. Chem. Soc.* **2013**, *135*, 10−13.
(33) Petrova, H.; Perez Juste, J.; Pastoriza-Santos, I.; Hartland, G. V.; Liz-Marzan, L. M.; Mulvaney, P. On the Temperature Stability of Gold Nanorods: Comparison between Thermal and Ultrafast Laser-Induced Heating. *Phys. Chem. Chem. Phys.* **2006**, *8*, 814−821.
(34) Albrecht, W.; Bladt, E.; Vanrompay, H.; Smith, J. D.; Skrabalak, S. E.; Bals, S. Thermal Stability of Gold/Palladium Octopods Studied *in Situ* in 3D: Understanding Design Rules for Thermally Stable Metal Nanoparticles. *ACS Nano* **2019**, *13*, 6522−6530.
(35) Antonello, A.; Della Gaspera, E.; Baldauf, J.; Mattei, G.; Martucci, A. Improved Thermal Stability of Au Nanorods by Use of Photosensitive Layered Titanates for Gas Sensing Applications. *J. Mater. Chem.* **2011**, *21*, 13074−13078.
(36) Weiner, R. G.; DeSantis, C. J.; Cardoso, M. B. T.; Skrabalak, S. E. Diffusion and Seed Shape: Intertwined Parameters in the Synthesis of Branched Metal Nanostructures. *ACS Nano* **2014**, *8*, 8625−8635.

https://dx.doi.org/10.1021/acsnano.0c07384
ACS Nano 2020, 14, 15953−15961

(37) Zhang, J.; Langille, M. R.; Mirkin, C. A. Photomediated Synthesis of Silver Triangular Bipyramids and Prisms: The Effect of PH and BSPP. *J. Am. Chem. Soc.* **2010**, *132*, 12502−12510.
(38) Willets, K. A.; Van Duyne, R. P. Localized Surface Plasmon Resonance Spectroscopy and Sensing. *Annu. Rev. Phys. Chem.* **2007**, *58*, 267−297.
(39) Mayer, K. M.; Hafner, J. H. Localized Surface Plasmon Resonance Sensors. *Chem. Rev.* **2011**, *111*, 3828−3857.
(40) Somarji, G. A.; Li, Y. *Introduction to Surface Chemistry and Catalysis*, 2nd ed.; Wiley: Hoboken, NJ, 2010.
(41) Reichelt, K. Nucleation and Growth of Thin Films. *Vacuum* **1988**, *38*, 1083−1099.
(42) Venables, J. A.; Spiller, G. D. T. Nucleation and Growth of Thin Films. *Surface Mobilities on Solid Materials: Fundamental Concepts and Applications*; NATO Advanced Science Institutes Series; Springer US: Boston, MA, 1983.
(43) Bauer, E.; van der Merwe, J. H. Structure and Growth of Crystalline Superlattices: From Monolayer to Superlattice. *Phys. Rev. B: Condens. Matter Mater. Phys.* **1986**, *33*, 3657−3671.
(44) Smith, J. D.; Woessner, Z. J.; Skrabalak, S. E. Branched Plasmonic Nanoparticles with High Symmetry. *J. Phys. Chem. C* **2019**, *123*, 18113−18123.
(45) Wang, Y.; Peng, H.-C.; Liu, J.; Huang, C. Z.; Xia, Y. Use of Reduction Rate as a Quantitative Knob for Controlling the Twin Structure and Shape of Palladium Nanocrystals. *Nano Lett.* **2015**, *15*, 1445−1450.
(46) Tao, A. R.; Habas, S.; Yang, P. Shape Control of Colloidal Metal Nanocrystals. *Small* **2008**, *4*, 310−325.
(47) Biacchi, A. J.; Schaak, R. E. The Solvent Matters: Kinetic *versus* Thermodynamic Shape Control in the Polyol Synthesis of Rhodium Nanoparticles. *ACS Nano* **2011**, *5*, 8089−8099.
(48) Berhault, G.; Bausach, M.; Bisson, L.; Becerra, L.; Thomazeau, C.; Uzio, D. Seed-Mediated Synthesis of Pd Nanocrystals: Factors Influencing a Kinetic- or Thermodynamic-Controlled Growth Regime. *J. Phys. Chem. C* **2007**, *111*, 5915−5925.
(49) Bower, M. M.; DeSantis, C. J.; Skrabalak, S. E. A Quantitative Analysis of Anions and PH on the Growth of Bimetallic Nanostructures. *J. Phys. Chem. C* **2014**, *118*, 18762−18770.
(50) Lide, D. R. *CRC Handbook of Chemistry and Physics: A Ready-Reference Book of Chemical and Physical Data*; CRC Press: New York, 1995.
(51) Gilroy, K. D.; Ruditskiy, A.; Peng, H.-C.; Qin, D.; Xia, Y. Bimetallic Nanocrystals: Syntheses, Properties, and Applications. *Chem. Rev.* **2016**, *116*, 10414−10472.
(52) Peng, X.; Pan, Q.; Rempel, G. L. Bimetallic Dendrimer -Encapsulated Nanoparticles as Catalysts: A Review of the Research Advances. *Chem. Soc. Rev.* **2008**, *37*, 1619−1628.
(53) Srinoi, P.; Chen, Y.-T.; Vittur, V.; Marquez, M. D.; Lee, T. R. Bimetallic Nanoparticles: Enhanced Magnetic and Optical Properties for Emerging Biological Applications. *Appl. Sci.* **2018**, *8*, 1106.
(54) Major, K. J.; De, C.; Obare, S. O. Recent Advances in the Synthesis of Plasmonic Bimetallic Nanoparticles. *Plasmonics* **2009**, *4*, 61−78.
(55) Mathurin, L. E.; Tao, J.; Xin, H.; Li, J.; Zhu, Y.; Chen, J. Dendritic Core-Frame and Frame Multimetallic Rhombic Dodecahedra: A Comparison Study of Composition and Structure Effects on Electrocatalysis of Methanol Oxidation. *ChemNanoMat* **2018**, *4*, 76−87.
(56) Chen, S.; Reggiano, G.; Thota, S.; Zhao, J. Au−Cu−Ag Nanorods Synthesized by Seed-Mediated Coreduction and Their Optical Properties. *Part. Part. Syst. Charact.* **2017**, *34*, 1600384.
(57) Kunz, M. R.; McClain, S. M.; Chen, D. P.; Koczkur, K. M.; Weiner, R. G.; Skrabalak, S. E. Seed-Mediated Co-Reduction in a Large Lattice Mismatch System: Synthesis of Pd−Cu Nanostructures. *Nanoscale* **2017**, *9*, 7570−7576.
(58) Weiner, R. G.; Skrabalak, S. E. Seed-Mediated Co-Reduction as a Route To Shape-Controlled Trimetallic Nanocrystals. *Chem. Mater.* **2016**, *28*, 4139−4142.
(59) Kobayashi, T.; Furukawa, Y.; Kikuchi, K.; Uyeda, H. On Twinned Structures in Snow Crystals. *J. Cryst. Growth* **1976**, *32*, 233−249.
(60) Kobayashi, T.; Furukawa, Y.; Takahashi, T.; Uyeda, H. Cubic Structure Models at the Junctions in Polycrystalline Snow Crystals. *J. Cryst. Growth* **1976**, *35*, 262−268.
(61) Gilroy, K. D.; Peng, H.-C.; Yang, X.; Ruditskiy, A.; Xia, Y. Symmetry Breaking during Nanocrystal Growth. *Chem. Commun.* **2017**, *53*, 4530−4541.
(62) Xia, X.; Xia, Y. Symmetry Breaking during Seeded Growth of Nanocrystals. *Nano Lett.* **2012**, *12*, 6038−6042.
(63) Sánchez-Iglesias, A.; Winckelmans, N.; Altantzis, T.; Bals, S.; Grzelczak, M.; Liz-Marzán, L. M. High-Yield Seeded Growth of Monodisperse Pentatwinned Gold Nanoparticles through Thermally Induced Seed Twinning. *J. Am. Chem. Soc.* **2017**, *139*, 107−110.
(64) Mu, C. F.; Yao, Q. Z.; Qu, X. F.; Zhou, G. T.; Li, M. L.; Fu, S. Q. Controlled Synthesis of Various Hierarchical Nanostructures of Copper Sulfide by a Facile Microwave Irradiation Method. *Colloids Surf., A* **2010**, *371*, 14−21.
(65) Wang, D.; Yu, D.; Shao, M.; Liu, X.; Yu, W.; Qian, Y. Dendritic Growth of PbS Crystals with Different Morphologies. *J. Cryst. Growth* **2003**, *257*, 384−389.
(66) Milliron, D. J.; Hughes, S. M.; Cui, Y.; Manna, L.; Li, J.; Wang, L.-W.; Paul Alivisatos, A. Colloidal Nanocrystal Heterostructures with Linear and Branched Topology. *Nature* **2004**, *430*, 190−195.

https://dx.doi.org/10.1021/acsnano.0c07384
ACS Nano 2020, 14, 15953−15961